Original Article

Developing a novel quasi-3D movable water phantom for radiation therapy workable in the magnetic resonance environment

Jian-Kuen Wu[1], Ting-Yen Lee[2], Min-Chin Yu[3], Ming-Chih Kuo[4], Wei-Chuan Chen[5], Yi-Cheng Hsiao[6], Yu-Jen Wang[7,8]

[1]Division of Radiation Oncology, Departments of Oncology, National Taiwan University Hospital, Taipei; [2]Department of Nuclear Medicine, National Taiwan University Hospital, Taipei; [3]Department of Radiation Oncology Taipei Medical University Hospital, Taipei; [4]Department of Medical Imaging, National Taiwan University Cancer Center, Taipei; [5]Department of Radiation Oncology, China Medical University Beigang Hospital, Yunlin; [6]Department of Medical Imaging, National Taiwan University Hospital, Taipei; [7]Department of Radiation Oncology, Fu Jen Catholic University Hospital, New Taipei City; [8]School of Medicine, College of Medicine, Fu Jen Catholic University, New Taipei City

Contributions: (I) Conception and design: JK Wu, MC Kuo, YJ Wang; (II) Administrative support: YJ Wang, JK Wu; (III) Provision of study materials or patients: JK Wu, YC Hsiao; (IV) Collection and assembly of data: JK Wu, TY Lee, WC Chen; (V) Data analysis and interpretation: TY Lee, MC Yu, YJ Wang; (VI) Manuscript writing: All authors; (VII) Final approval of manuscript: All authors.

Correspondence to: Yu-Jen Wang, MD, LLB, PhD. Department of Radiation Oncology, Fu Jen Catholic University Hospital, New Taipei City; School of Medicine, College of Medicine, Fu Jen Catholic University, No. 510, Zhongzheng Rd., Xinzhuang Dist., New Taipei City 242. Email: 138697@mail.fju.edu.tw.

Background: The use of magnetic resonance linear accelerators (MR-LINACs) for clinical treatment has opened up new possibilities and challenges in the field of radiation oncology. However, annual quality assurance (QA) is relatively understudied due to practical considerations. Thus, to overcome the difficulty of measuring the dose with a small water phantom for TRS-398 or TG-51 in all external beam radiation treatment unit environments, such as MR compatibility, we designed a remote phantom with a three-axis changeable capacity for QA.

Methods: The designed water phantom was tested under an MR environment. The water phantom system comprised of three parts: a phantom box, a dose measurement tool, and a PMD401 drive system. The UNIDOSE universal dosimeter was used to collect beam data. The manufacturer's developer tools were utilized to position the measurement. To ensure magnetic field homogeneity, a distortion phantom was prepared using sixty fish oil capsules aligned radially to distinguish the oil and free air. The phantom was scanned in both the MR simulator and computed tomography (CT), and the acquired images were analyzed to determine the position shift.

Results: The dimensions of the device are 30 cm in the X-axis, 20 cm in the Y-axis, and 17 cm in the Z-axis. Total cost of materials was no more than $10,000 US dollars. Our results indicate that the device can function normally in a regular 1.5 T MR environment without interference from the magnetic field. The water phantom's traveling speed was found to be approximately 5 mm/s with a position difference confined within 6 cm intervals during normal use. The distortion test results showed that the prepared MR environment has uniform magnetic field homogeneity.

Conclusions: In this study, we constructed a prototype water phantom device that can function in an MR simulator without interference between the magnetic field and electronic components. Compared to other commercially available MR-LINAC water phantoms, our device offers a more cost-effective solution for routine monthly QA. It can shorten the duration of QA tests and relieve the burden on medical physicists.

Keywords: Water phantom; radiation therapy; magnetic resonance (MR); low cost; movable

Submitted Feb 15, 2023. Accepted for publication Aug 25, 2023. Published online Sep 13, 2023.
doi: 10.21037/qims-23-189
View this article at: https://dx.doi.org/10.21037/qims-23-189

Introduction

The use of magnetic resonance linear accelerators (MR-LINACs) for clinical treatment has opened up new possibilities and challenges in the field of radiation oncology (1). MR-LINAC is increasingly being used in routine clinical practice (2,3). To ensure radiotherapy (RT) quality, periodic quality assurance (QA), including daily, monthly, and annually QA, such as absolute dose measurement, beam profile establishment, and energy check, was developed to ensure the precision of the treatment beam (4). However, annual QA is relatively understudied due to practical considerations, leading to a lack of research in this area for MR-LINAC (5,6).

Before starting patient treatment, perform extensive QA on the treatment plans, including isocenter location, imaging and patient handling system, and LINAC stability is critical for the quality of patient care of RT (7). It usually verifies the accuracy of the planned dose distribution by testing it in a water phantom, which simulates human soft tissue. However, commercial water phantoms for the MR-LINAC environment are limited due to geometric and mechanical problems, and setting up a water phantom on an MR-LINAC is challenging due to the strong magnet field and the absence of a light field and optical distance indicator (8).

Recently, two models of QA products such as THALES 3D MR SCANNER and BEAMSCAN® MR 3D water phantom (PTW, Freiburg, Germany) have developed commercial water phantoms for MR-LINAC but they are too expensive to limit its use to do commission and annual QA (9). To address this need, we plan to design a low-cost, easy for daily or monthly QA homemade motorized water phantom using readily available materials.

Methods

Phantom module design

These characteristics are mandatory for a QA phantom design of MR-LINAC: (I) no ferromagnetic components; (II) lightweight and compact design; and (III) motors should not affect the MR imaging (MRI) and unaffected by the magnetic field. Thus, we customized the MR-compatible motor driver, which could drive the water tank under the MR environment without inference. The motor driver was made of ceramic piezo, with traveling-wave piezoelectric effects (10,11), and the motor could move smoothly in a quasi-stepwise way under a magnet environment.

The homemade MR distortion phantom was scanned under a computed tomography (CT) machine and MR machine with the same center. To study the effect of the presence of a 1.5 T magnetic field, all of the tests were repeated with the distortion phantom in the MRI scanners Siemens MAGNETOM Aera 1.5 T (Siemens Healthcare, Erlangen, Germany). The scanning plan was delivered by the clinical 1.5 T MR environment SIGNA Artist MRI (GE Medical Systems, Milwaukee, WI, USA), and CT images were acquired from the Philips Brilliance Big Bore (Philips Medical Systems, Cleveland, OH, USA). Both image data were reconstructed by the built-in software with 1.5-mm-thick slices. The MR sequence included localizer, T1-weighted, and T2-weighted images. The setting of the CT acquisition was referred to clinical use. After scanning, the displacement of the fusion image was measured to analyze the MR homogeneity.

To reach the objective of affordability, we restrict the total cost of materials to no more than $10,000 US dollars.

QA experiment

Compatibility and homogeneity were tested in the MR environment and the system-related distortion were also checked. Geometric distortion is an inevitable problem when objects are used in MR environments due to imperfect MR system hardware and changes in the magnetic field (12). The heterogeneity of the magnetic field might affect the image quality and the further planning dose of RT. Thus, in this study, we highlighted the image distortion experiment while acquiring the image data.

The distortion phantom was made of polymethylmethacrylate (PMMA), which contained several fish oil capsule radical placements. The purpose of designing 60 fish oil capsules is to provide more standard geometric structures and to easily differentiate the interface between air and oil. Anatomic landmark point-based measurements were performed between the corresponding MR and CT images to quantify the distortions with CT considered the undistorted ground

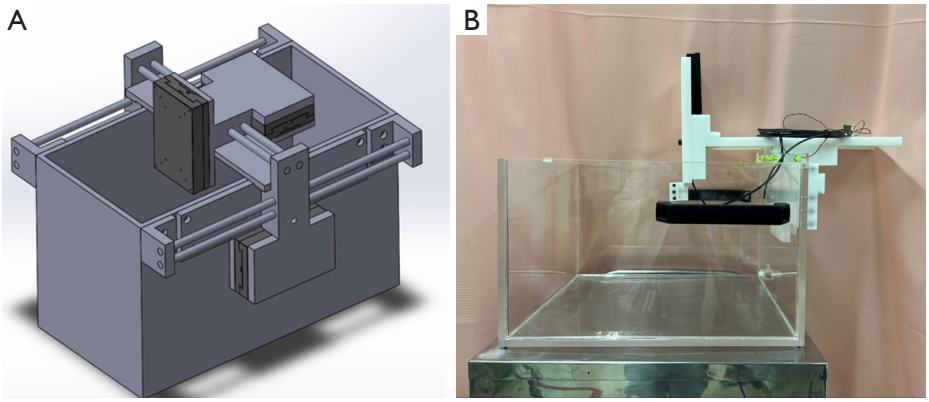

Figure 1 The configuration of the phantom. (A) The design drawing of the phantom. (B) The finished product of the phantom.

truth. In the QA experiment, the distortion phantom was placed in front of the water phantom, presenting as a whole entity, which provided the X-Y positioning correction, preventing the X-Y direction distortion resulted from 1.5 T magnet field.

For dosimetry measurement, the experiment was done in the tomotherapy environment (Tomotherapy Hi-Art System, Madison, WI, USA). The UNIDOSE universal dosimeter (Farmer type, PTW30013) with MP3-T Semiflex chamber holding device was used for output measurement. For water phantom scan, the A1SLMR ion chamber (https://www.standardimaging.com/) was set up in treatment room and connected to the channel 2; while the A17 ion chamber was set up in control room and connected the channel 3, which was used for pseudo-reference. The both mentioned ion chamber were supplied with −300 V, and the TomoElectrometer 8 channel electrometer was used to supply the charge.

The TEMS 2 software was applied for processing beam profile analysis under Window 7 system. The output beam profile would undergo re-processing to eliminate the digital signal spike.

Results

Homemade MR-compatible water phantom

The low-cost MR-compatible water phantom consists following parts.

Phantom box

The water phantom system contained three parts: phantom box, dose measurement tools, and drive system. The phantom box was made of 8 mm-thick PMMA, with inner dimensions of 40×20×20 cm^3 (*Figure 1A,1B*).

Drive system

For the drive system, we referred to the past review about the piezoelectric-related linear movement, trying to follow the principle that had been proposed. The homemade motor was made by local manufacturers, and all of the components, including toothed wheels, arms, and other related kits, were made of plastic or PMMA. The stator section of the piezoelectric linear motor constructed with a meander-line structure. A series of bimorph actuators is arranged in a line, and the neighboring actuators are linked through connectors between them.

The odd and even actuators were driven by phase-split alternating current (AC) power to generate a traveling wave. The traveling wave was transferred to the carriage via gear teeth mounted on the meander-line structure and created the linear movement.

The bimorph actuator consists of a piece of metal sandwiched between two pieces of ceramic. Deformation occurs when the piezoelectric ceramics are driven by AC power.

$$u_{pz} = \frac{1}{2} s_{11}^{E} (\sigma_1)^2 + d_{31} E_3 \sigma_1 + \frac{1}{2} \varepsilon_{33}^{T} E_3^2 \quad [1]$$

$$u_m = \frac{1}{2} s_{11}^{m} (\sigma_1^m)^2 \quad [2]$$

where s_1 and σ_1 are the strain and the stress of the ceramics in the 1 direction, respectively; E_3 and D_3 are the electric field and the dielectric displacement of piezoelectric ceramic in the 3 direction, respectively; s_{11}^{E} is the mechanical stiffness of piezoelectric ceramic given encountered with constant electric field in the 1 direction; d_{31} is the

piezoelectric constant in the 31 direction; ε_{33}^{T} is the dielectric of piezoelectric ceramic given by constant stress in the 3 direction; s_1^m is the strain of the metal in the 1 direction; s_{11}^m is the mechanical stiffness of the metal; σ_1^m is the stress of the metal in the 1 direction. The strain energy method is used to compute the deformation of the bimorph (13). The index u_{pz} represents the energy of the piezoelectric ceramics, and the index u_m represents the energy of the metal.

Assuming that a force P_F is applied to the bimorph, the moment is given by:

$$\mathrm{M}(z)=\frac{1}{2}P_F w_{pz}\left(L_{pz}-z\right)^2 \quad [3]$$

w_{pz} is the width of the piezoelectric ceramics; L_{pz} is the length of the piezoelectric ceramics. The external and the three-axes direction placement of motor driver system are shown in *Figures 2,3A,3B*. Overall, an MR-compatible trolley was used in this experiment for storage and equipment transportation (*Figure 3C*).

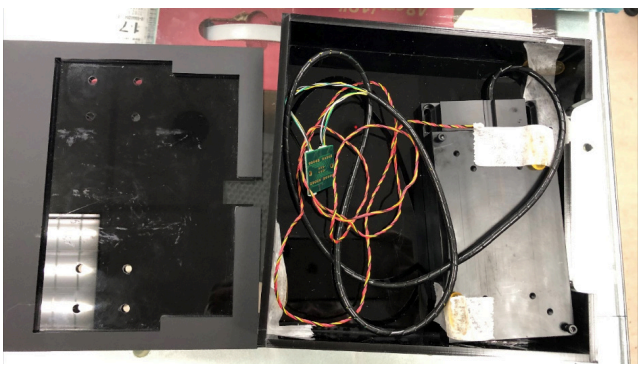

Figure 2 The motor driver system.

Control system

These 2 N piezo motors combine with PMD401 positioning control using piezo slides. The X and Y axes have both manual and electric interfaces. The board is powered with a 48 V direct current (DC) power supply (±5%). Current consumption at 48 V is 0.02 A when the motor is stopped and a maximum of 0.4 A when the motor is running at maximum speed. The save command Y32 is used to store the axis address (and other settings) in flash memory, or pinouts and connectors, connects to the host via universal serial bus (USB) [virtual communication port (COM port)]. Use the data terminal software of choice and send commands in American Standard Code for Information Interchange (ASCII) format. Standard USB mini-B connector for connection to personal computer. Upon driver installation, a Future Technology Devices International (FTDI) virtual COM port will open for serial communication.

A target command will enter "target mode" (closed loop), and a stop command will end "target mode". An open loop run command will end "target mode" as well. The closed loop normally runs every 1 ms, except for some slow serial synchronous interface encoders where the target loop iterates every 2 ms. There is no error checking for 32-bit encoder position rollover, but there are position limits that can be used to prevent this situation in closed loops.

A high level of "analog enable" activates "analog". The amplifier enables (AENs) the signal from the motion controller to connect to the AEN input and unpark the motor at a high level. Alternatively, connect the AEN signal from the motion controller to "analog enable" and use a separate signal for park/unpark control.

The serial peripheral interface (SPI) signals are AC-terminated at 120 Ω in series with 1 nF capacitors. Single-

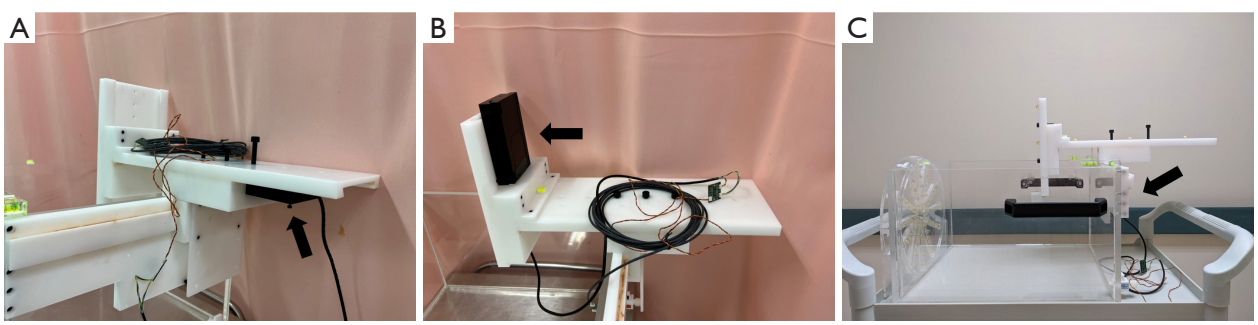

Figure 3 The motor driver with three-direction arrangement. (A) The arrangement in X-direction. (B) The arrangement in Y-direction. (C) The arrangement in Z-direction. The black arrows pointed out the different position of the motor driver, which could deliver the water phantom in one-direction movement.

ended signals may be used if all inverted inputs are tied together and buffered with a 100 nF capacitor.

Connect "analog enable" to ground connection (GND) or leave it unconnected. The AENs the signal from the motion controller to connect to the AEN input and unpark the motor at a high level. The SPI master out, slave in (SPI_MOSI) input controls the motor speed. The motor will stop when the input SPI data are =0. The PMD301 expects regular speed updates and will stop the motor if no SPI data have been received for approximately 10 ms. The 16-bit signed SPI data give linear speed control (stepping rate). Note that the motor step is not constant, and a position sensor (encoder) is necessary for feedback to the motion controller. More details could be found at the technical manual (Piezo LEGS® Controller PMD401).

Homemade distortion phantom

The customized distortion phantom was prepared with sixty radically placed fish oil capsules (*Figure 4*). The cylindrical container was made of 0.5-cm-thick PMMA with a height of 3 cm, and the bottom was a 30 cm diameter concentric circle with a hollow diameter of 4 cm. The fish oil capsules aimed to provide more standard geometric structures and to differentiate the interface between air and oil easily, which were placed in radical alignment.

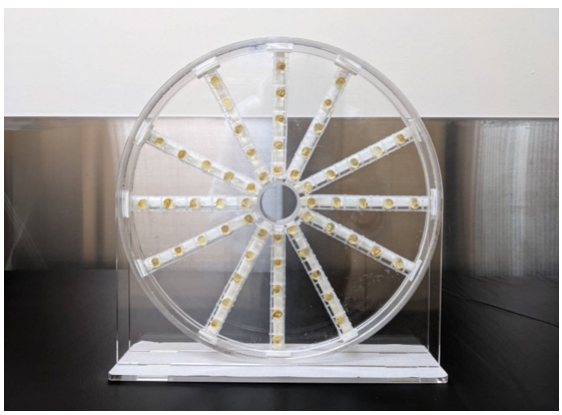

Figure 4 The structure of distortion phantom.

MR homogeneity

To ensure MR uniformity, the distortion phantom was scanned under MR and CT separately. The results showed that the displacement of MR images could be confined within 1 mm based on CT images. The fusion image shown in *Figure 5* demonstrates that the image shift could be ignored with naked eye discrimination.

Compatibility

The integration of MR distortion phantom and the QA water phantom was placed on the MR compatible trolly (*Figure 3C*) and scanned under the MR environment (*Figure 6A*).

The results showed that the water phantom was operated smoothly in the MR simulator without any artifacts on the images (*Figure 6B*). The high-intensity magnet field did not influence the motor of the water phantom. With normal use, the moving speed of the phantom could reach 5 mm/s with a position difference confined to 1 mm under the MR simulator.

Availability

To test the availability, the water phantom equipped with

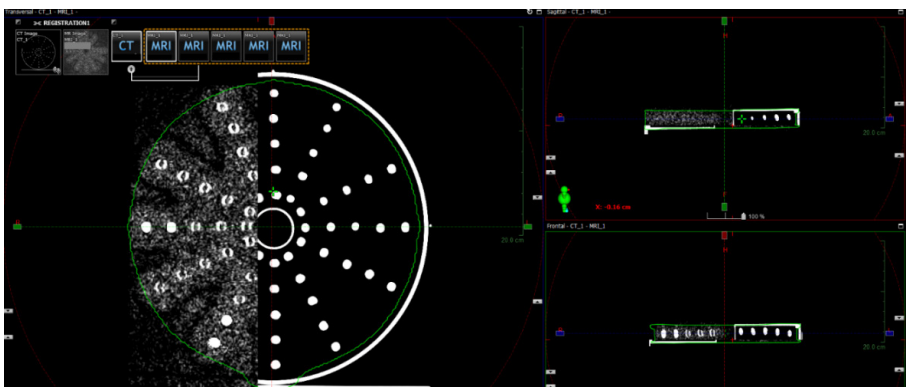

Figure 5 The fusion MR and CT image of distortion phantom. CT, computed tomography; MRI, MR imaging; MR, magnetic resonance.

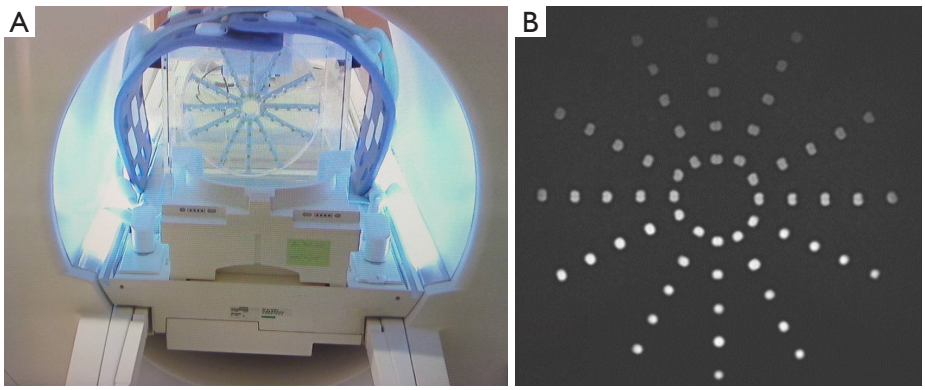

Figure 6 The execution of QA water phantom under MR environment. (A) The scanning situation of QA phantom in MR machine. (B) The MR image of distortion phantom. QA, quality assurance; MR, magnetic resonance.

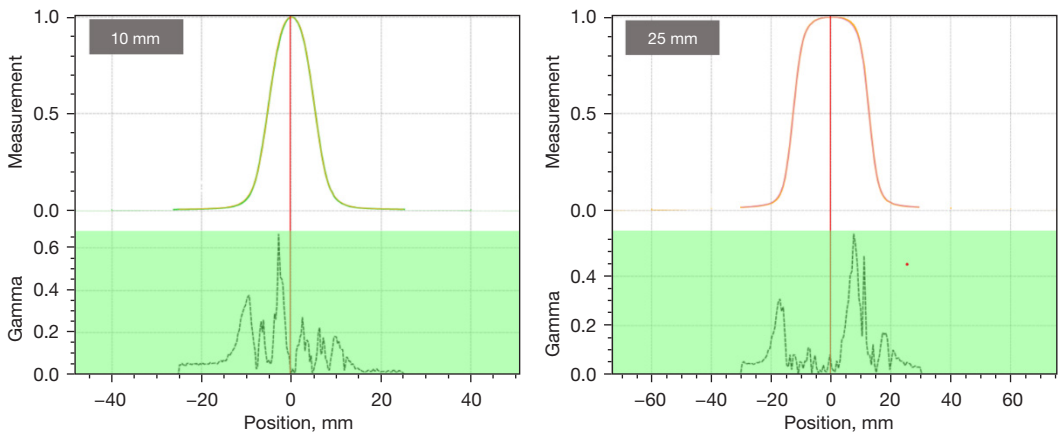

Figure 7 The beam profile of QA water phantom. The designed phantom was scanned by 6 MV photon beam with y=10 mm (left) and y=25 mm (right) under QA mode without gantry rotation. QA, quality assurance; MV, megavoltage.

ion chamber was scanned under the Tomotherapy Hi-Art System. The 1.5-depth gamma beam profile of the prototype water tank was shown in *Figure* 7. The results showed that the water tank could work normally and the gamma index was accepted reasonable for current condition.

Besides, the percent depth dose (PDD) of the water phantom was depicted in *Figure 8*. The 14/10 ratio was 0.757, comparing to reference (0.756, acquiring from annual QA record) presented the extraordinary dose distribution. Limit to temporary motor driver moving range, the PDD calculation only could be executed with 14/10 ratio instead of 20/10 protocol.

Given the above, a novel piezoelectric-driven motor system that can run in an MRI environment has been developed. The design also shows the great flexibility, which can be applied in different commercial MR-linac systems such as Tomo™ Hi-Art system, Varian Halcyon™, Unity™ Elekta, and MRIdian-LINAC ViewRay. Noted that the size of water tank should be customized to fit the various field size of different MR-LINAC system (ViewRay 0.35 T: 0.2×0.425–27.4×24.1 cm^2; Unity 1.5 T: 0.5×0.5–57.4×22 cm^2).

Discussion

This 30 cm size multi-function MR compatible phantom could be a solution to meet the regulation of TG 51 (14) and TRS 398 (15) concomitantly and cost effectively phantom (less than US $10,000) to help physicists to do monthly QA easily. Its weight is lighter, suitable for the most of the radiation therapy external beam system, and could do radiation energy check, PDD check, and a part of

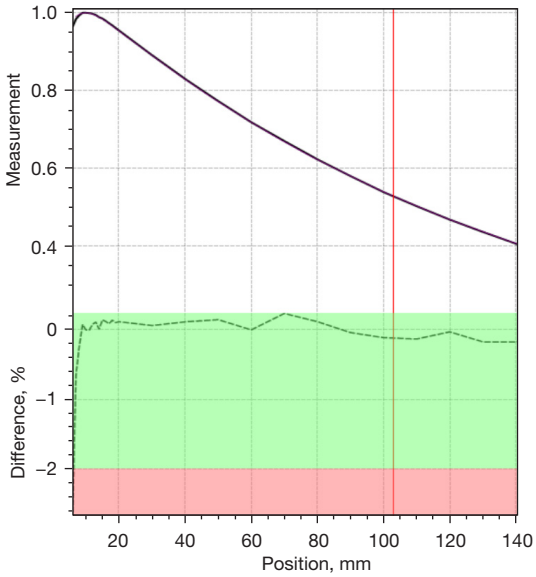

Figure 8 The PDD of QA water phantom. PDD, percent depth dose; QA, quality assurance.

beam profiles.

With better soft tissue contrast and radiation-free characteristics, MRI has been commonly used in medical diagnosis. The concept of the combination of a LINAC and MR image has also become popular, which provides better image quality and biological and functional information, increasing the treatment accuracy. In addition, compared to a conventional LINAC equipped with cone beam CT, MR-LINAC provided on-time images during treatment without irradiation exposure. Currently, accumulating research on the clinical application of MR-LINAC has shown the new trend of this device. Meanwhile, with increasing interest, there is a need to focus on the regular check-ups and maintenance package of MR-LINAC. However, limited to a strong magnet field, QA of the MR-LINAC was challenging because of magnet field interference (6).

In this study, piezoelectric materials were introduced and applied to a motor system to avoid magnet interference and to do actuate and simultaneously measure (16). The power was delivered from the mutual interaction of piezoelectric ceramics. With the AC current supplied, the wriggling compartments pushed the gear teeth and then moved the carried object without producing any current. This study first tests the availability of the designed motor in the MR environment and further apply it to the annual QA of MR-LINAC. The results demonstrated that the homemade motor with a water phantom could be used safely in the MR environment in the compatibility test. Here, due to the safety and the cost of performing the experiment in MR-LINAC, we performed this experiment in the MR-simulator. To ensure the MR uniformity and correct the image distortion, we also designed a homemade distortion phantom, which was made up of several fish-oil capsules in radical alignment. To our knowledge, this two-dimensional (2D) point-like phantom was primarily introduced for MR homogeneity. In our experiment, the distortion phantom was scanned under CT and MR machine. While CT images presented as a template for MR images correlation, the neatly arranged targets could be somehow needless. Also, the fusion of the two images could further process the X-Y plane distortion map and be managed in excel work sheet. As the measured PDD statistics of beam scan entered in, through the mentioned map, the slight distortion could be automatically corrected. Noted that the distortion phantom could be used alone, or cooperated with different functions phantom, measuring the image contrast or image uniformity.

After ensuring the feasibility in homogeneous MR environment, we draw the comparison between our device and current marketed water phantom, THALES 3D MR SCANNER (https://www.lap-laser.com/products/thales-3d-mr-scanner/) and BEAMSCAN® MR 3D water phantom (https://www.ptwdosimetry.com/en/application-pages/mr-guided-radiotherapy/), by set-up time, traveling velocity, measuring range, step size, and measuring accuracy. First, it took us 15 min to set up a water phantom, as same as those devices in the devices mentioned above. Next, the traveling speed of the homemade motor with a water phantom could reach 5 mm/s. Although the marketed water phantom showed better traveling speeds (30 mm/s) than our device, the slower velocity also meets the most clinical need (fine: 1 mm/s; coarse: 6 mm/s) (17). The delivering range of designed water phantom was 170 mm for independent axis. In mentioned devices, 370×373×237 mm^3 of measuring range in THALES 3D MR SCANNER was reported; 568×145×355 and 408×248×355 mm^3 for Elekta and ViewRay respectively in BEAMSCAN® MR 3D water phantom. To lower the cost, one-axis motor was designed with reducing by one-third expenditure. With repeating the one-axis motor manipulation, we could measure more than 568 mm in one direction. Meanwhile, we also could measure volumetric parameter with three-dimension adjust. In comparison of other mechanical parameters, our water phantom provided the modest step size of

0.1 mm as same as aforementioned machines reported. Besides, THALES 3D MR SCANNER showed the great measuring accuracy (±0.25 mm), however, piezoelectric-drive motor could not achieve the high accuracy under the speedy movement due to its physical characteristics. In fact, in our experiment, the real position could be showed timely with the installation of optical linear encoder.

To meet the goal of the affordable, the one-axis movement was manufactured as a prototype, which could only perform linear movement but not multiple axes movement at the same time. As a result, in further experiments, we tended to change the component in the device and improve it so that it could move freely and measure the volumetric dose profile, shortening the procedure time. Developing affordable medicine and medical LINACs is an issue to be discussed (18,19). As our previous experience on multi-function and low-cost phantom innovation (20,21), to reach maximum benefit with minimum resources meets clinical needs could be a way to help people to approach modern RT.

In addition, we plan to build a position feedback system. In the study, we manipulated the drive motor and measured the distance artificially. To improve the precise location of the water phantom, the computed feedback system was installed into the device, providing the exact location of the ion chamber. With the stable operation of the device and successful pre-experiment result, the high-level motor could be induced in, providing the farther measuring range and load increment.

Finally, during the experiment, we also observed that the appearance of the water phantom should be remodeled. In our opinion, the position of the drainage of the phantom should be changed from the side face to bottom so that more space of the scanning bed in MR could be released. Additionally, considering the measurement accuracy, the size of the water phantom should be customized for different uses. The MR images of the smaller phantom with the coil covered tightly presented better image resolution than the larger phantom. To acquire the best result, we need to choose the favorable size of the water tank to meet the different tasks in the QA procedure. In the future, we expect to design a smaller phantom that can meet the needs of the clinic, showing portability and easy-to-use characteristics (22).

Based on the problem we posed, this prototype still had a long way to go. In the future, we plan to upgrade the fundamental functions, such as traveling speed, three-orientation movement, and positioning feedback system, and improve the water phantom appearance to maximize the efficiency of the QA water phantom. We expected that with this designed system, the duration of the QA test will be shortened and relieve the MR-LINAC users' burden. In summary, the pilot experiment showed a novel concept that the innovative carriage device could play its effectiveness in the annual QA of MR-LINAC.

Conclusions

We have built a low-cost, innovated MR-compatible water phantom for annual QA of MR-LINAC machine. To the best of your knowledge, our innovation is first to combine the affordable materials to do multi-function and MR-compatible phantom and will help the MR based RT in the future.

Acknowledgments

The authors would like to thank all colleagues who contributed to this study and the technique support from National Taiwan University Hospital. We would like to thank the QIMS's inhouse language editor for native language expression improvement. In addition, we are grateful to two anonymous reviewers and the editor for their comments.

Funding: The work was supported by the research project of Fu Jen Catholic University Hospital (No. PL201908001V).

Footnote

Conflicts of Interest: All authors have completed the ICMJE uniform disclosure form (available at https://qims.amegroups.com/article/view/10.21037/qims-23-189/coif). The authors have no conflicts of interest to declare.

Ethical Statement: The authors are accountable for all aspects of the work in ensuring that questions related to the accuracy or integrity of any part of the work are appropriately investigated and resolved. The materials and methods used in this study did not involve any patients or animals. Therefore, the ethical approval and informed consent are not applicable.

References

1. Hall WA, Paulson E, Li XA, Erickson B, Schultz C, Tree A, Awan M, Low DA, McDonald BA, Salzillo T, Glide-Hurst CK, Kishan AU, Fuller CD. Magnetic resonance linear accelerator technology and adaptive radiation therapy: An overview for clinicians. CA Cancer J Clin 2022;72:34-56.
2. Tocco BR, Kishan AU, Ma TM, Kerkmeijer LGW, Tree AC. MR-Guided Radiotherapy for Prostate Cancer. Front Oncol 2020;10:616291.
3. Winkel D, Werensteijn-Honingh AM, Eppinga WSC, Intven MPW, Hes J, Snoeren LMW, Visser SA, Bol GH, Raaymakers BW, Jürgenliemk-Schulz IM, Kroon PS. Dosimetric feasibility of hypofractionation for SBRT treatment of lymph node oligometastases on the 1.5T MR-linac. Radiother Oncol 2021;154:243-8.
4. Mittauer KE, Dunkerley DAP, Yadav P, Bayouth JE. Characterization and longitudinal assessment of daily quality assurance for an MR-guided radiotherapy (MRgRT) linac. J Appl Clin Med Phys 2019;20:27-36.
5. Chen X, Ahunbay E, Paulson ES, Chen G, Li XA. A daily end-to-end quality assurance workflow for MR-guided online adaptive radiation therapy on MR-Linac. J Appl Clin Med Phys 2020;21:205-12.
6. Roberts DA, Sandin C, Vesanen PT, Lee H, Hanson IM, Nill S, Perik T, Lim SB, Vedam S, Yang J, Woodings SW, Wolthaus JWH, Keller B, Budgell G, Chen X, Li XA. Machine QA for the Elekta Unity system: A Report from the Elekta MR-linac consortium. Med Phys 2021;48:e67-85.
7. Chera BS, Jackson M, Mazur LM, Adams R, Chang S, Deschesne K, Cullip T, Marks LB. Improving quality of patient care by improving daily practice in radiation oncology. Semin Radiat Oncol 2012;22:77-85.
8. Woodings SJ, de Vries JHW, Kok JMG, Hackett SL, van Asselen B, Bluemink JJ, van Zijp HM, van Soest TL, Roberts DA, Lagendijk JJW, Raaymakers BW, Wolthaus JWH. Acceptance procedure for the linear accelerator component of the 1.5 T MRI-linac. J Appl Clin Med Phys 2021;22:45-59.
9. Ferrer C, Huertas C, García D, Sáez M. Dosimetric characterization of a novel commercial plastic scintillation detector with an MR-Linac. Med Phys 2023;50:2525-39.
10. Ting Y, Chen LC, Li CC, Huang JL. Traveling-wave piezoelectric linear motor Part I: the stator design. IEEE Trans Ultrason Ferroelectr Freq Control 2007;54:847-53.
11. Ting Y, Li CC, Chen LC, Yang CM. Traveling-wave piezoelectric linear motor part II: experiment and performance evaluation. IEEE Trans Ultrason Ferroelectr Freq Control 2007;54:854-60.
12. Neylon J, Cook KA, Yang Y, Du D, Sheng K, Chin RK, Kishan AU, Lamb JM, Low DA, Cao M. Clinical assessment of geometric distortion for a 0.35T MR-guided radiotherapy system. J Appl Clin Med Phys 2021;22:303-9.
13. Smits JG, Choi W. The constituent equations of piezoelectric heterogeneous bimorphs. IEEE Trans Ultrason Ferroelectr Freq Control 1991;38:256-70.
14. Almond PR, Biggs PJ, Coursey BM, Hanson WF, Huq MS, Nath R, Rogers DW. AAPM's TG-51 protocol for clinical reference dosimetry of high-energy photon and electron beams. Med Phys 1999;26:1847-70.
15. Huq MS, Hwang MS, Teo TP, Jang SY, Heron DE, Lalonde RJ. A dosimetric evaluation of the IAEA-AAPM TRS483 code of practice for dosimetry of small static fields used in conventional linac beams and comparison with IAEA TRS-398, AAPM TG51, and TG51 Addendum protocols. Med Phys 2018. [Epub ahead of print]. doi: 10.1002/mp.13092.
16. McPherson T, Ueda J. A force and displacement self-sensing piezoelectric MRI-compatible tweezer end effector with an on-site calibration procedure. IEEE/ASME Transactions on Mechatronics 2013;19:755-64.
17. Althof V, van Haaren P, Westendorp R, Nuver T, Kramer D, Ikink M, Bel A, Minken A. A quality assurance tool for helical tomotherapy using a step-wedge phantom and the on-board MVCT detector. J Appl Clin Med Phys 2012;13:3585.
18. Dosanjh M, Aggarwal A, Pistenmaa D, Amankwaa-Frempong E, Angal-Kalinin D, Boogert S, et al. Developing Innovative, Robust and Affordable Medical Linear Accelerators for Challenging Environments. Clin Oncol (R Coll Radiol) 2019;31:352-5.
19. Lentz R, Benson AB 3rd, Kircher S. Financial toxicity in cancer care: Prevalence, causes, consequences, and reduction strategies. J Surg Oncol 2019;120:85-92.
20. Wu JK, Chen SH, Hsu FM, Liao SH, Wang YJ. Design of a motion simulation system to assist respiratory gating for radiation therapy. Med Dosim 2021;46:360-3.

21. Wu JK, Yu MC, Chen SH, Liao SH, Wang YJ. Low cost multifunctional 3D printed image quality and dose verification phantom for an image-guided radiotherapy system. PLoS One 2022;17:e0266604.
22. Palm A, LoSasso T. Influence of phantom material and phantom size on radiographic film response in therapy photon beams. Med Phys 2005;32:2434-42.

Cite this article as: Wu JK, Lee TY, Yu MC, Kuo MC, Chen WC, Hsiao YC, Wang YJ. Developing a novel quasi-3D movable water phantom for radiation therapy workable in the magnetic resonance environment. Quant Imaging Med Surg 2023;13(12):7731-7740. doi: 10.21037/qims-23-189

